ORIGINAL PAPER



Pulse transmission and acoustic non-reciprocity in a granular channel with symmetry-breaking clearances

Qifan Zhang^{1,2} • Wei Li¹ · John Lambros³ · Lawrence A. Bergman³ · Alexander F. Vakakis²

Received: 29 June 2019

© Springer-Verlag GmbH Germany, part of Springer Nature 2019

Abstract

Granular media composed of ordered arrays of discrete spherical granules have attracted considerable attention due to their highly nonlinear and discontinuous dynamics and acoustics that enable passively adaptive and tailorable properties. In this work we numerically study nonlinear pulse propagation in a two-dimensional (2D) granular channel composed of a main homogeneous lattice with several pairs of side granules. Depending on the direction of pulse transmission in the main lattice, a periodic series of symmetry-breaking clearances alter the topology of this 2D granular network. The rotational dynamics of the individual granules, as well as dissipative effects due to friction between granules (and their boundaries) and inherent material damping, are proven to play a significant role in the acoustics of the granular channel. This is demonstrated by comparing the theoretical predictions of this work to experimental measurements of the same system reported earlier. Moreover, the strong nonlinearity of this system in synergy with the topological asymmetry introduced by the clearances passively breaks acoustic reciprocity. To this end, a detailed study of pulse transmission in the 2D granular channel is performed, and it is shown that by simply changing the direction of pulse transmission it is possible to switch the nonlinear acoustics from Nesterenko solitary pulses to strongly decaying propagating pulses. In the latter case there is continuous and irreversible transfer of energy from the main propagating pulse to the side granules, which act, in essence, as nonlinear energy absorbers. This work highlights the important role that (even small) geometric imperfections (asymmetries) may play on the acoustics of 2D granular media.

Keywords Non-reciprocity · 2D granular lattice · Geometric effects · Solitary pulses

1 Introduction

Tunable wave propagation in granular media composed of ordered or packed arrays of discrete linearly elastic particles (granules) in Hertzian contact has attracted considerable

Electronic supplementary material The online version of this article (https://doi.org/10.1007/s10035-019-0982-7) contains supplementary material, which is available to authorized users.

☐ Qifan Zhang hustzqf@hust.edu.cn

Published online: 23 December 2019

- School of Naval Architecture and Ocean Engineering, Huazhong University of Science and Technology, Wuhan 430074, China
- Department of Mechanical Science and Engineering, University of Illinois at Urbana-Champaign, Urbana, IL 61801, USA
- Department of Aerospace Engineering, University of Illinois at Urbana-Champaign, Urbana, IL 61801, USA

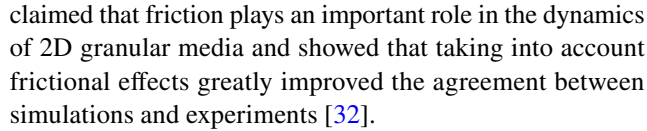
attention from both theoretical and practical points of view. Nesterenko performed pioneering research in the field of nonlinear wave propagation in one-dimensional (1D) ordered granular media and proved analytically, numerically and experimentally the existence of a new type of spatially localized and shape preserving strongly nonlinear solitary waves [1, 2] with speed depending on amplitude, and thus exhibiting passive tunability with respect to energy. Due to their highly tunable and tailorable dynamic properties, initially uncompressed ordered granular media are capable of forming and transmitting a broad range of stress waves, such as propagating solitary pulses [1, 3-9], traveling waves [10, 3-9]11], a mixture of solitary and nonlinear shear waves [12], and transient breathers [13–15]. In addition, these nonlinear acoustic media, which have been characterized as "acoustic vacua" due to their purely energy-dependent speed of sound (in contrast to the constant speed of sound in classical linear acoustic waveguides), can support tunable (with energy) pass bands, intense nonlinear energy exchanges and "energy



explosions" [16], targeted energy transfers and passive wave redirection [14], and strongly non-reciprocal acoustics [17]. Due to these unique acoustical features, ordered granular media have been considered for various potential applications and in novel engineering devices, e.g., as nonlinear acoustic lenses [18, 19], shock and energy absorbing layers [20–22], passive acoustic filters [23] and acoustic switches [24].

The highly nonlinear nature of the Hertzian and collisional interactions between granules makes it possible for non-reciprocal pulse propagation in the presence of asymmetry or structural disorder in 1D ordered granular media. Boechler et al. [25] experimentally demonstrated a mechanism for tunable rectification based on bifurcations and chaos in the nonlinear acoustics of a statically compressed one-dimensional array of granules containing a light mass defect. As a result of the defect, vibrations at selected frequencies caused dynamical instability and a subsequent jump from regular to quasi-periodic and chaotic states with broadband frequency. Depending on the position of the defect relative to the point of actuation, the system's response could be switched from a high-amplitude transmitting state to a low-amplitude non-transmitting one. Cui et al. [26] proposed a granular device composed of a 23-bead granular chain and a conical rod. Excitation from different sides of the assembly gave rise to vastly different output responses indicating that the frequency-preserved non-reciprocal acoustic propagation in a lower frequency range in that system could be experimentally realized.

Despite the growing amount of research in this field, there are only a few studies of non-reciprocal acoustics of twodimensional (2D) granular media in the current literature. This may be attributed to the complicated nature of granular mechanics in 2D settings, especially when the granules not only interact through Hertzian forces but also exhibit frictional effects. Based on the open source molecular mechanics package LAMMPS (Large-scale Atomic/Molecular Massively Parallel Simulator [27]), Amnaya et al. [28] numerically studied the impact-induced wave propagation in closely packed 2D granular media and observed the propagation of 2D solitary waves. Leonard [29] investigated pulse propagation in 2D hexagonal granular assemblies and found that a propagating pulse decays as it propagates through that medium. Li et al. [30] studied a similar 2D hexagonally packed granular system with multiple granules being impacted, and noted that the impact excitations yielded two distinct solitary waves of the same amplitude and a trailing train of weaker solitary waves with smaller velocities. However, typically the 2D models considered in previous studies only included Hertzian normal contact interactions between granules and did not incorporate dissipation mechanisms associated with damping and particularly frictional contact. Yet, in some other works, Yang [31] and Goldenberg [32]



For example, Pal et al. [33] numerically and experimentally studied pulse propagation in a 2D granular channel. Geometric tolerances in that system altered the network topology depending on the point of actuation, and the nonlinear acoustical behavior could be switched from rapidly decaying pulses to unaltered solitary pulses. The work described in [33] provides the main motivation for the present study, since it can be considered as an interesting system for breaking acoustical non-reciprocity. However, the simplifying assumptions in the numerical model employed in [33] give rise to deviations of the computational predictions from the experimental measurements; these discrepancies are reexamined in the present work after removing some of these simplifications in the model.

In this paper we numerically study the non-reciprocal acoustics of the 2D granular channel first introduced in [33]. Apart from developing a more accurate computational model that accounts for the rotational dynamics of the individual granules, as well as the frictional dissipation caused by these rotational effects, neither of which was considered in [33], herein emphasis is placed on the study of nonreciprocal pulse transmission in this system. The remainder of this manuscript is structured as follows. In Sect. 2, we present the governing equations of the 2D inclined granular channel. In Sect. 3, we revisit the results of [33] and numerically study the tunable pulse propagation in two different topological configurations of the granular channel, now taking into account the rotational and frictional effects in the individual granules. The efficacy of a new mathematical model that accounts for these effects is validated by comparing its predictions with the experimental measurements of [33] and through additional energy considerations. The key factors that affect the strongly nonlinear acoustics in this system are also discussed. In Sect. 4, we employ the mathematical model to study acoustic non-reciprocity in an extended version of the inclined granular channel possessing a symmetry-breaking periodic series of geometric clearances. We show that the geometric clearances induce strong non-reciprocity in the nonlinear acoustics, and propose measures for its quantification. Finally, in Sect. 5 we summarize the main findings of this work and discuss some potential practical applications.

2 Theoretical modeling

In this work we consider 2D ordered granular networks composed of multiple identical spherical linearly elastic granules with modulus E, Poisson's ratio v, mass m and



radius R. Each of the considered granular lattice networks is arranged within the confines of two parallel rigid walls on an inclined plane, thus forming an inclined granular channel. Given that the inclination angle of the channel is sufficiently small, assumptions are made that gravity does not affect the nonlinear acoustics of the granular network (although it does affect the static topology and gives rise to the asymmetric clearances in the network) and that no precompression exists. Such a granular channel is depicted in Fig. 1a, composed of a main homogeneous granular lattice (indicated by the blue axial granules) and several symmetrically placed side granules (indicated by red). Assuming that there exist periodic tolerances between the granules of the main lattice and the side ones, when the channel is inclined by a fixed angle φ there will be a periodic series of clearances between the side granules and some of their neighboring axial granules of the main lattice. Moreover, given that the side granules are assumed to be in perfect contact with their neighboring granules situated in the main lattice, a geometric asymmetry in the configuration of the granular channel will result. In addition, it is assumed that all side granules are in perfect contact with the corresponding rigid side walls of the channel and that no pre-compression exists in the system; this is shown in the top view of Fig. 1b.

It is interesting to note that the nonlinear acoustics of this inclined granular channel differ qualitatively depending on the path of pulse transmission. Indeed, referring to Fig. 1 we note that, following the application of an external impulse to one of the boundaries and depending on the *direction* of the pulse transmission (i.e., upstream, or downstream, cf. Fig. 1a), the topological configuration of the granules of the system changes, and this is anticipated

to affect the resulting acoustics. This is discussed in more detail in Sect. 3.

Apart from the translational granular motions considered in previous studies [33-36], the rotational degrees-of-freedom of the granules as well as friction effects should also be included in this type of 2D setting, since not all Hertzian interactions are expected to occur through the mass centers, resulting in friction torques acting on the granules. This point was demonstrated clearly by Yang and Sutton in [31], where it was shown that failure to do so would lead to erroneous results. Accordingly, an angular velocity ω is defined for each granule, which is taken as positive when the granule rotation is counterclockwise (cf. Fig. 2), and a Coulomb friction model is assumed to model the frictional effects. Finally, two additional simplifying assumptions are made, namely, (i) that the inclination angle is sufficiently small so that, although it is gravity that gives rise to the asymmetric geometric clearances, it nevertheless does not affect the nonlinear acoustics of the granular channel; and (ii) that there is no friction between the granules and the base of the channel (that would introduce complicated 3D effects which are neglected in this work).

A new 2D granular interaction model was developed for the present study having as its basis (but not being identical to) a similar prior model developed by Yang and Sutton in [31]. The following formulation assumes 2D (planar) motions (cf. Fig. 1b), so any non-planar effects are ignored. We begin by describing the *normal contact force* between two neighboring granules, e.g., granules *i* and *j*, as shown in Fig. 2. Each granule is of spherical shape and composed of a linear elastic material. Assuming small deformations and imposing some additional simplifying assumptions that ensure the validity of the model as in [37], we may consider each granule as a point mass at its geometric center and

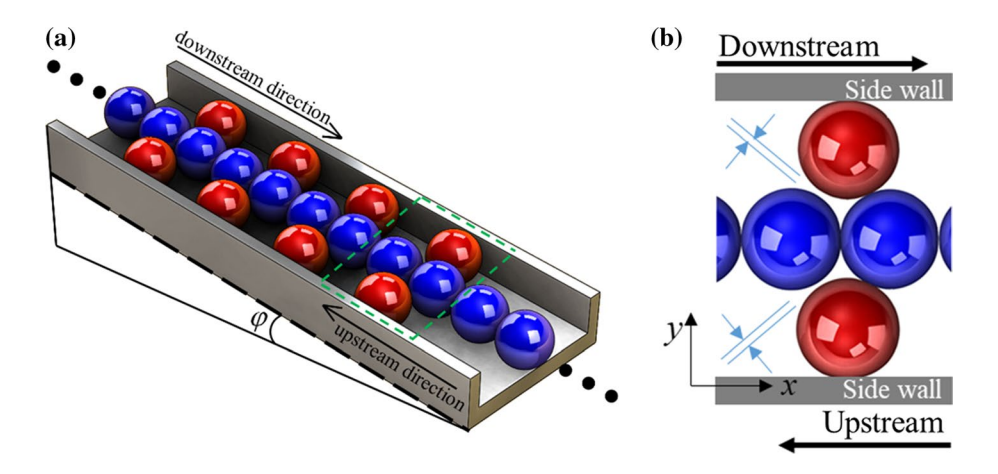
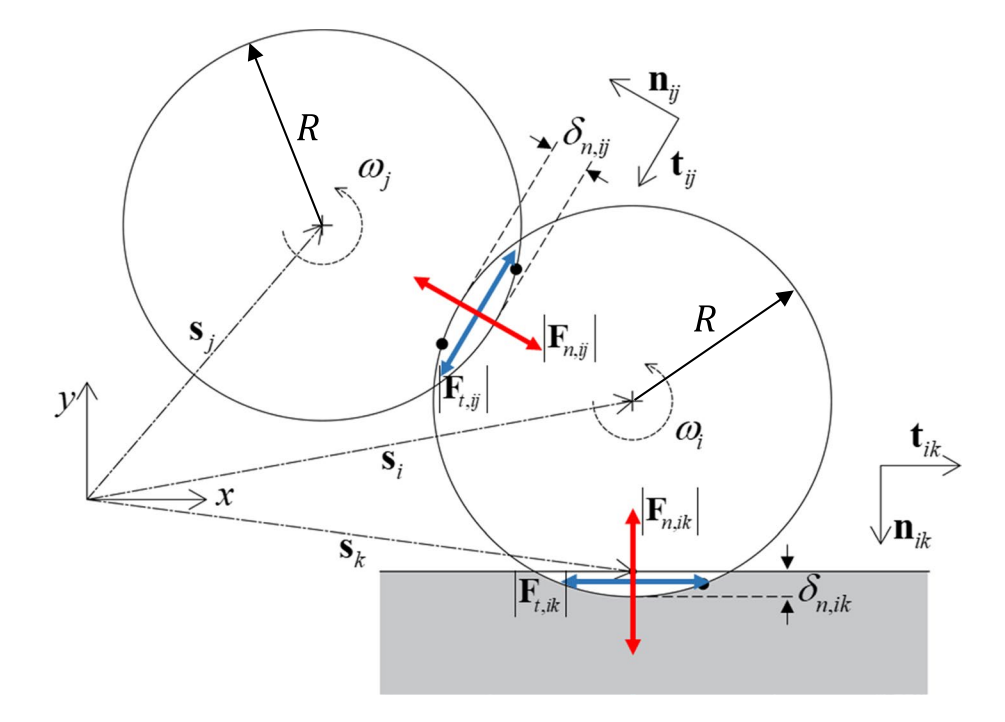


Fig. 1 Schematic of the 2D granular channel considered in this work, with blue axial granules composing the main homogeneous 1D granular lattice and red granules being symmetrically placed causing the geometric tolerances due to gravity by the inclination angle φ : a ste-

reographic view, and **b** top view showing the symmetry-breaking tolerances; the model follows the experimental fixture used in [33], all spherical granules have identical geometrical and material properties, and only 2D planar motions (in the *xy*-plane) are considered



Fig. 2 Schematic of two identical interacting granules under compression, with one of the granules having an additional possible interaction with a rigid side wall; the subscripts i, j and k denote granule or wall indices, the subscripts n and t denote normal and tangential force components, respectively, and the possibility of granule rotations is taken into account through the instantaneous angular velocities ω_i and ω_i



describe the normal interactions between two contacting granules in terms of a nonlinear (Hertzian) spring situated in parallel to a viscous damper, and acting along an axis connecting their centers [37–39]. We note that the viscous damper models the dissipation force due to the material damping of the granules. Then, the normal component of the contact force acting on granule i by granule j is given by,

$$\mathbf{F}_{n,ij} = -A_{ij}\delta_{n,ij}^{3/2}\mathbf{n}_{ij} + \gamma_{n,ij}\dot{\delta}_{n,ij}\mathbf{n}_{ij}$$
 (1)

where \mathbf{n}_{ij} is the normal unit vector pointing from the center-of-mass of the *i*th granule to the *j*th (cf. Fig. 2), $\delta_{n,ij}$ is the deformation of the distance between centers under compressive contact (where before deformation of this distance was equal to 2R), and $\dot{\delta}_{n,ij}$ is the corresponding deformation velocity. The first term in (1) represents the elastic contact force based on the Hertzian contact law, with the contact coefficient A_{ij} given by,

$$A_{ij} = \frac{\sqrt{2RE}}{3(1 - v^2)} \tag{2}$$

The second term in (1) is the damping part with the damping coefficient $\gamma_{n,ij}$ expressed as [31],

$$\gamma_{n,ij} = \alpha_n (mA_{ij})^{1/2} \delta_{n,ij}^{1/4}$$
 (3)

where α_n is an empirical constant related to the coefficient of restitution. Note that the damping coefficient increases with normal compression $\delta_{n,ij}$.

Given the position vectors \mathbf{s}_i and \mathbf{s}_j pointing from the origin of the inertial reference frame to the center-of-mass of

the *i*th and *j*th granules (cf. Fig. 2), respectively, the transient position vector of the *j*th granule relative to the *i*th is given by $\mathbf{s}_{ij} = \mathbf{s}_j - \mathbf{s}_i$, with the normal unit vector in that direction given by $\mathbf{n}_{ij} = \mathbf{s}_{ij} / |\mathbf{s}_{ij}|$. Accordingly, the normal deformation between these two granules can be expressed as,

$$\delta_{n,ij} = \max(2R - \left| \mathbf{s}_{ij} \right|, 0) \ge 0 \tag{4}$$

in order to take into account the possibility of zero compressive deformation in the absence of any compression between granules, i.e., during granule separation; hence, no tensile normal forces are allowed. Similarly, the relative velocity vector of the *j*th granule with respect to the *i*th granule is $\dot{\mathbf{s}}_{ij} = \dot{\mathbf{s}}_j - \dot{\mathbf{s}}_i$, where overdot represents the differentiation with respect to time. Hence, taking into account (4), the normal deformation velocity is defined as,

$$\dot{\delta}_{n,ij} = \begin{cases} \dot{\mathbf{s}}_{ij} \cdot \mathbf{n}_{ij}, & \delta_{n,ij} > 0 \\ 0, & \delta_{n,ij} = 0 \end{cases}$$
 (5)

with dot denoting the inner product between vectors.

Considering now the *tangential contact forces* during granular interactions, clearly these forces are due to nonnegligible granule rotations and give rise to frictional effects. Such frictional contact forces introduce additional strongly nonlinear and non-smooth effects in the granular acoustics, that is, in addition to the Hertzian contact nonlinearities originating due to compression of neighboring granules. Adopting the Coulomb friction model, the tangential contact force acting on the *i*th granule by the *j*th, is approximately modeled by,



$$\mathbf{F}_{t,ij} = \mu \left| \mathbf{F}_{n,ij} \right| \operatorname{sign}(\dot{\delta}_{t,ij}) \mathbf{t}_{ij}$$
(6)

where \mathbf{t}_{ij} is the tangential unit vector in the direction defined by the cross product of the angular velocity (pseudo) vector and the normal vector \mathbf{n}_{ij} (cf. Fig. 2), μ is the coefficient of friction, and $\dot{\delta}_{t,ij}$ is the tangential relative velocity of the contact point in the *j*th granule with respect to that of the *i*th (cf. Fig. 2),

$$\dot{\delta}_{t,ii} = \left[(\dot{\mathbf{s}}_i - \dot{\mathbf{s}}_i) - R(\omega_i + \omega_i) \mathbf{t}_{ii} \right] \cdot \mathbf{t}_{ii}$$
 (7)

In (7) it is assumed that the granules are rotating with instantaneous angular velocities ω_i and ω_j , respectively. Note that the positive direction of the tangential relative velocity is defined by the direction of \mathbf{t}_{ij} , so that the direction of the frictional force $\mathbf{F}_{t,ij}$ exerted on the granules is always opposite to the relative motion.

The contact force between a granule and a rigid side wall is similar to the contact forces between interacting granules discussed above. Indeed, considering the previous formulation and replacing the *j*th granule by the *k*th contact point with a rigid side wall (cf. Fig. 2)—determined by the normal projection of the center of *i*th granule on the wall—the resulting normal deformation and approaching velocity between the *i*th granule and its neighboring side wall are given by,

$$\delta_{n,ik} = \max(R - |\mathbf{s}_k - \mathbf{s}_i|, 0) \tag{8}$$

$$\dot{\delta}_{n,ik} = \begin{cases} (\dot{\mathbf{s}}_k - \dot{\mathbf{s}}_i) \cdot \mathbf{n}_{ik} = -\dot{\mathbf{s}}_i \cdot \mathbf{n}_{ik}, & \delta_{n,ik} > 0 \\ 0, & \delta_{n,ik} = 0 \end{cases}$$
(9)

Note that in this case, the *k*th contact point on the wall is a particle-specific point which "moves" with the *i*th granule so that the unit vector $\mathbf{n}_{ik} = (\mathbf{s}_k - \mathbf{s}_i)/|\mathbf{s}_k - \mathbf{s}_i|$ is always normal to the wall. Accordingly in (9), $\dot{\mathbf{s}}_k$ is always orthogonal to \mathbf{n}_{ik} and hence irrelevant to the equation. The expression (1) of the normal component of the interaction force in this case still holds, while the normal Hertzian contact coefficient should be modified in order to account for the different geometry such that,

$$A_{ik} = \frac{2\sqrt{RE}}{3(1 - v^2)} \tag{10}$$

With regard to the tangential component of the contact force, the relationship (6) still applies, while the tangential relative velocity of the contact point of the *i*th granule relative to the side wall is now approximated by,

$$\dot{\delta}_{t,ik} \approx \left[-\dot{\mathbf{s}}_i - R\omega_i \mathbf{t}_{ik} \right] \cdot \mathbf{t}_{ik} \tag{11}$$

Taking into account that, in the 2D granular channels considered herein, the *i*th granule can be potentially in simultaneous contact with more than one neighboring granule and the side wall, the resultant contact force acting on the *i*th granule is the summation of the above-mentioned contact forces. Accordingly, the governing equations of motion for the *i*th granule can be expressed as,

$$m\ddot{\mathbf{s}}_{i} = \sum_{j} (\mathbf{F}_{n,ij} + \mathbf{F}_{t,ij}) + \sum_{k} (\mathbf{F}_{n,ik} + \mathbf{F}_{t,ik})$$

$$I\dot{\boldsymbol{\omega}}_{i} = R \sum_{j} (\mathbf{n}_{ij} \times \mathbf{F}_{t,ij}) + R \sum_{k} (\mathbf{n}_{ik} \times \mathbf{F}_{t,ik})$$
(12)

where I is the mass moment of inertia of the spherical granule. Assembling the equations of motion of all granules provides the system of equations of motion of the entire granular channel. In this study, this system of equations is solved for zero initial conditions and an impulse applied to either of the boundaries of the main homogeneous lattice (cf. Fig. 1) using a fourth-order Runge–Kutta scheme with a sufficiently small time step Δt compared to the characteristic time scales of the granule dynamics and the pulse propagation in the granular channel.

In addition, we will be interested in energy computations following the application of the impulse. To this end, the instantaneous kinetic and potential energies of the entire granular channel are expressed as,

$$K.E. = \sum_{i} \left(\frac{1}{2} m |\dot{\mathbf{s}}_{i}|^{2} + \frac{1}{2} I \omega_{i}^{2} \right)$$

$$P.E. = \sum_{i} \left[\sum_{j} \left(\frac{1}{5} A_{ij} \delta_{n,ij}^{5/2} \right) + \sum_{k} \left(\frac{2}{5} A_{ik} \delta_{n,ik}^{5/2} \right) \right]$$
(13)

where the summations are carried out over all granules. Moreover, the energies dissipated by viscous and friction effects up to time instant t, $W_{\text{viscous}}(t)$ and $W_{\text{friction}}(t)$, respectively, are computed through the integrals,

$$W_{\text{viscous}}(t) = -\int_{0}^{t} \left[\sum_{i} \left(\sum_{j} \left(\gamma_{n,ij} \dot{\delta}_{n,ij} \mathbf{n}_{ij} \cdot \dot{\mathbf{s}}_{i} \right) + \sum_{k} \left(\gamma_{n,ik} \dot{\delta}_{n,ik} \mathbf{n}_{ik} \cdot \dot{\mathbf{s}}_{i} \right) \right) \right] d\tau$$

$$W_{\text{friction}}(t) = -\int_{0}^{t} \left[\sum_{i} \left(\sum_{j} \left(\mathbf{F}_{t,ij} \cdot (\dot{\mathbf{s}}_{i} + R\omega_{i} \mathbf{t}_{ij}) \right) + \sum_{k} \left(\mathbf{F}_{t,ik} \cdot (\dot{\mathbf{s}}_{i} + R\omega_{i} \mathbf{t}_{ik}) \right) \right) \right] d\tau$$

$$(14)$$



Note that a dissipative force can do only negative work on the system. Hence a minus sign is applied in Eqs. (14) such that the expressions for the dissipated energies $W_{\rm viscous}(t)$ and $W_{\rm friction}(t)$ are always non-negative. Clearly, at each time instant the summation of the instantaneous potential and kinetic energies of all granules, as well as the total dissipated energies up to that time instant, should remain equal to the impulsive energy imparted to the system at time instant t=0+ (based on conservation of total energy) expressed by,

$$\underbrace{(K.E. + P.E.)}_{T.E.} + \underbrace{(W_{damp} + W_{friction})}_{W} \equiv \text{Input energy}$$
(15)

This energy criterion will be assessed at each time instant in the computational studies to follow as a measure of the accuracy of the numerical simulations.

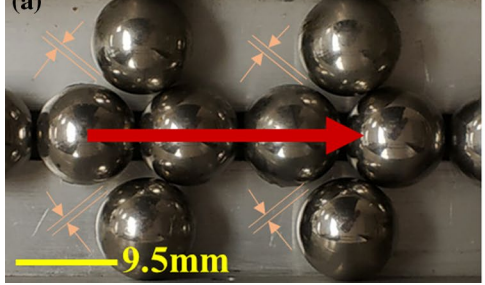
3 Direction-dependent pulse propagation in the granular channel

In this section, nonlinear pulse propagation in a granular channel introduced by Pal et al. [33], which has similar configuration to that shown in Fig. 1, is discussed. The granular network presented in Figs. 3 and 4 is composed of a certain number of axial granules (forming the main homogeneous

granular lattice) with a varying number of pairs of side granules symmetrically placed along the sides of the main lattice. The angle θ denotes the angle between the axial direction and the line connecting the centers of a side granule and its contacting axial granule (cf. Fig. 4). Assuming that all granules are identical, when $\theta > 60^{\circ}$, a periodic series of clearances exists between the side granules and one of their neighboring axial granules, such that each side granule is initially in contact with only one axial granule and the sidewall of the inclined granular channel. A steel support is installed at the right (lower) boundary (cf. Figs. 1a, 4a) to prevent the main granular lattice from rolling away [33] and is regarded as a fixed rigid wall in our numerical model. The upper boundary of the main granular lattice is free.

This system was first studied experimentally by applying an impulsive load at either of the boundaries of the main homogeneous granular lattice [33]. Following the application of the load, pulse propagation is initiated in the system, which, however, depends on the direction of energy transmission. This is highlighted in Figs. 3 and 4, where the *downstream* and *upstream* configurations of the granular channel with five pairs of side granules are considered. The experiments performed in [33] for the downstream configuration considered 21 axial granules, whereas the experiments for the upstream configuration were carried out with 18 granules. The numerical model considered in this section follows the experimental setups. Moreover, in this work we

Fig. 3 Experiment setup of the granular channel [33]: a downstream configuration and b upstream configuration; the clearances in the two configurations are highlighted (the arrows show the direction of primary pulse propagation)



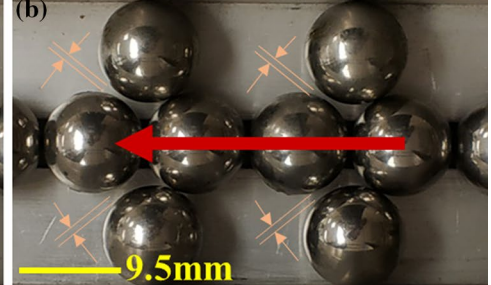
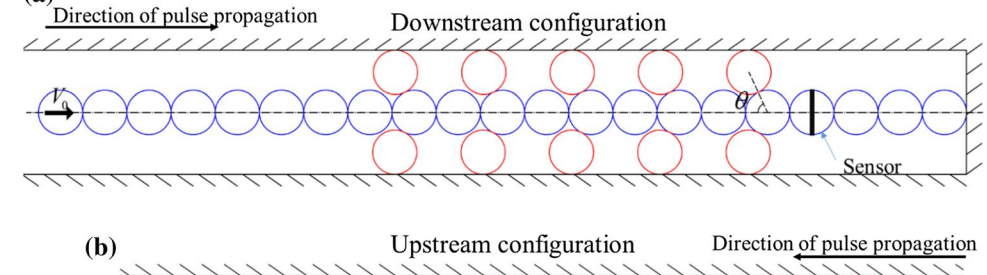
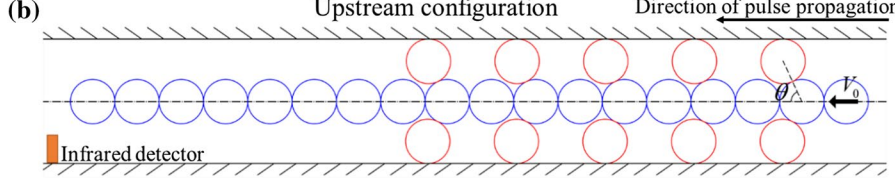


Fig. 4 Schematic of the topology of the granular channel with 5 pairs of side granules studied in [33]: a downstream configuration with 21 axial granules and **b** upstream configuration with 18 axial granules; a piezoelectric force sensor is embedded in the 18th granule in the downstream configuration, and an infrared detector is placed close to the upper boundary of the main lattice in the upstream configuration to measure the escape velocity of the end granule







consider only primary pulse transmission, i.e., only the initial wave front generated following the application of the impulsive load at the boundary, and we are not interested in any reflections coming from the boundaries.

For an impulsive load applied at the upper boundary, downstream pulse transmission occurs, and the topological configuration of the system is depicted in Figs. 3a and 4a; whereas, for excitation at the lower boundary, upstream pulse transmission occurs and the altered topological configuration is depicted in Figs. 3b and 4b. The key difference between these two configurations concerns the different topologies of the clearances between the side granules and their neighboring axial granules. That is, for downstream pulse propagation, due to the existence of the clearances the axial granules do not make contact with their neighboring side granules until after the primary pulse has been transmitted downstream. However, for upstream pulse propagation, the axial granules make contact and interact with the side granules during the arrival of the primary pulse and before it is transmitted upstream. As a result, downstream primary pulse propagation in the main granular lattice is unaffected by the side granules, whereas upstream primary pulse propagation does get affected by the side granules.

Pal et al. [33] performed a series of experimental measurements of primary pulse transmission in these two configurations for different numbers of pairs of side granules. Given an impulsive load at a boundary, a rapidly decaying primary pulse propagating along the main lattice was experimentally observed for the upstream configuration, while the downstream configuration was shown to support the propagation of Nesterenko solitary pulses as in a simple homogeneous granular lattice [1, 3]. Pal et al. [33] also performed numerical simulations with the model that accounted only for normal granular interactions but ignored rotational, friction and damping effects. As a result, their numerical predictions overestimated the experimental measurements. In the present work we revisit the systems studied in [33] and, by including rotational and frictional effects, we achieve better agreement between numerical predictions and experimental measurements, quantifying the importance of including these effects.

The developed numerical model closely follows the experimental granular channel studied in [33] where the granules were arranged in an slightly inclined channel $(\varphi \approx 2^{\circ})$ with a smooth Teflon holder ramp on the bottom and confining steel walls on both sides. The spherical granules considered were made of stainless steel with a diameter of 2R = 9.525 mm, Young's modulus E = 200 GPa, density $\rho = 7670 \text{ kg/m}^3$, and Poisson's ratio $\nu = 0.3$. An impact velocity of $V_0 = 0.62$ m/s along the axial direction was applied at the axial granule on either boundary, ensuring elastic deformations throughout the pulse propagation. Correspondingly, a total simulation time window of 0.4 ms with a sufficiently small time step $\Delta t = 2 \times 10^{-9}$ s is employed, which has been shown to be sufficient to fully capture the nonlinear pulse propagation of interest. As an approximation, the same empirical damping constant and friction coefficient used in [31], $\alpha_n = 6.313 \times 10^{-3}$ and $\mu = 0.099$, are applied, providing the effect of structural damping, and the granule-to-granule and granule-to-wall friction forces, respectively. Note that by assuming a small angle of inclination ($\varphi \approx 2^{\circ}$), the component of gravity parallel to the slope (the x-direction in Fig. 1b) is estimated to be about 1.2×10^{-3} N, or about four orders of magnitude smaller than the estimated interaction forces during pulse propagation; hence, gravity effects are neglected. The friction between the granules and the bottom holder of the channel is also neglected so that planar acoustics are studied. It is clear that due to symmetry the axial granules composing the main lattice will move axially, despite the rotational and frictional effects of the side granules, provided that the clearances in the system are periodic and symmetrically placed on both sides of the main lattice.

The position angle θ (cf. Fig. 4) is set to 61°, so that the time scale of the primary pulse propagation along the main lattice is much smaller compared with the time it takes for a side granule to cover the clearance and make contact with its neighboring axial granule during downstream or upstream pulse transmission. Equivalently, it is ensured that within the time window considered in the simulations, the side granules can interact only with a single neighboring axial granule.

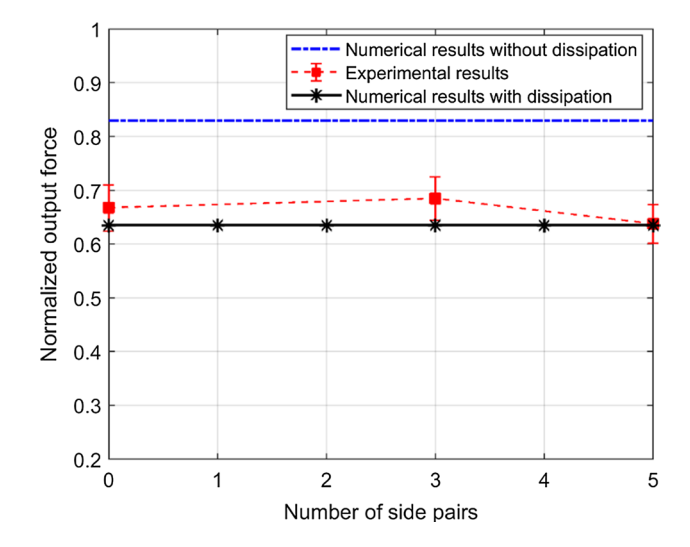


Fig. 5 Peak axial force at the 18th granule normalized by the peak of the impulsive force acting on the first granule for downstream pulse transmission: Numerical predictions obtained in [33] without including any viscous, friction or rotational effects (dashed-dotted line), compared to the experimental measurements [33] (dashed line with standard deviation error bars) and the numerical predictions of the current model that includes viscous, friction and rotational effects (solid line)



In the plot of Fig. 5 we depict the normalized peak axial force at the 18th axial granule for downstream pulse transmission and different numbers of side granule pairs. In this configuration a primary Nesterenko solitary pulse is transmitted in the main granular lattice following the application of the impulsive load since, due to the configuration of the clearances, the side granules do not affect primary

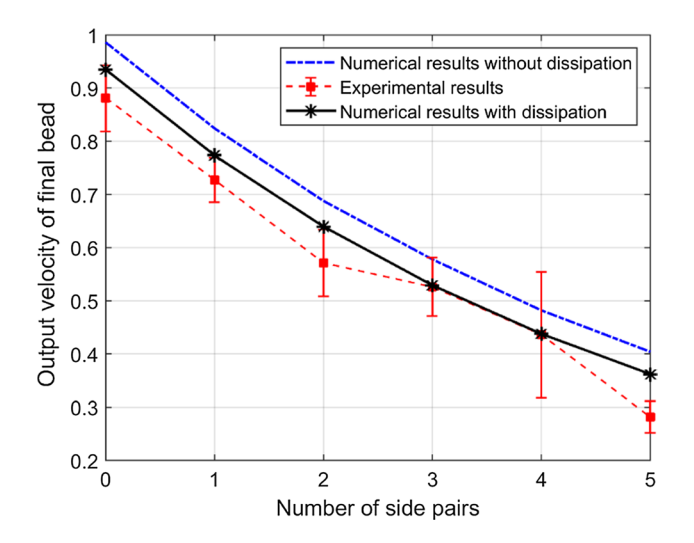


Fig. 6 Output velocity of the first granule normalized by the velocity $V_0 = 0.62$ m/s of the granule where the impulse is applied (upstream pulse transmission): Numerical predictions obtained in [33] without including any viscous, friction or rotational effects (dashed-dotted line) compared to the experimental measurements [33] (dashed line with standard deviation error bars) and the numerical predictions of the current model that includes viscous, friction and rotational effects (solid line)

pulse transmission. In the plot we compare the numerical predictions obtained in [33] without including any viscous, friction, or rotational effects in the experimental measurements [33] and to the numerical predictions of the current model that includes viscous, friction and rotational effects. It is noted that the current model significantly improves the accuracy of the numerical modeling and predicts normalized force peaks that are much closer (within the range of the error bars) of the experimental measurements.

In Fig. 6 we consider the normalized velocity of the first granule of the main lattice in the upstream configuration with different numbers of side granule pairs. Again, the predictions of the current numerical model are compared to the experimental measurements and the dissipation-less and rotation-less numerical predictions of [33]. Our numerical results better approximate the experimental measurements, with remaining discrepancies likely due to unmodeled effects, e.g., the frictional effects on the granules due to the Teflon base. We note that in this case the side granules drastically affect the propagation of the primary pulse in the main lattice, rapidly removing energy from it, and thus resulting in a decaying propagating pulse. Hence, the output normalized velocity decreases rapidly with increasing number of side granule pairs, confirming that the side granules indeed play a significant role in the nonlinear acoustics in the upstream configuration. It is interesting to note that there are significant rotations of the side granules, giving rise to friction torques.

To gain better insight into the nonlinear acoustics of pulse propagation for both configurations, the simulation results for the system with 5 pairs of side granules (cf. Fig. 4) using

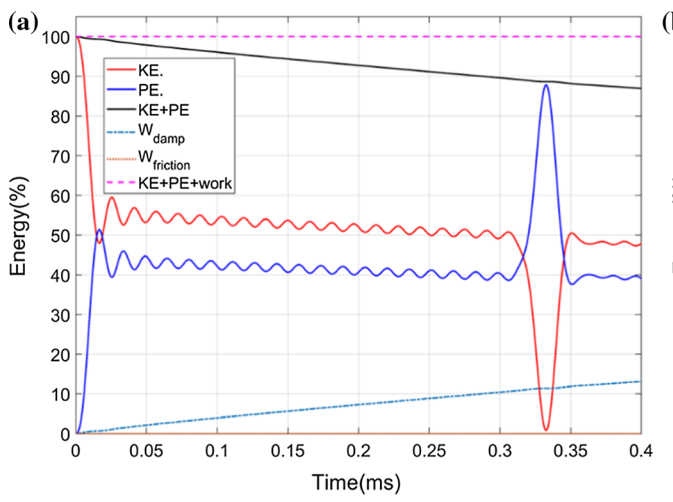
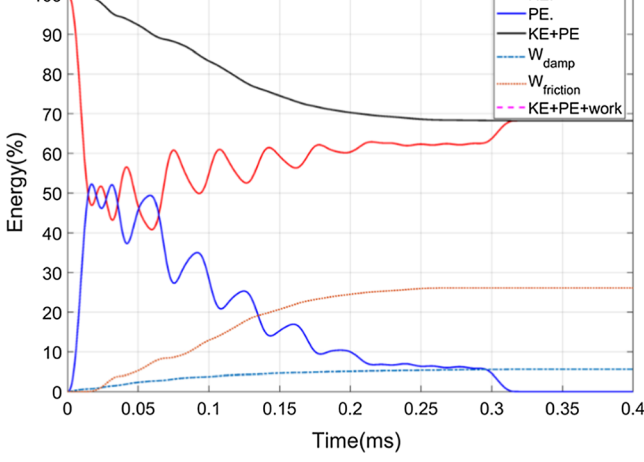


Fig. 7 Instantaneous energy partition in the impulsively excited granular channel for ${\bf a}$ downstream and ${\bf b}$ upstream pulse transmission, including kinetic energy K.E. (red solid curve), potential energy P.E. (blue solid line), dissipated energy due to viscoleastic effects $W_{\rm damp}$ (dashed-dotted line), and dissipated energy due to friction $W_{\rm friction}$



(dotted line); the energy components are normalized with respect to the input energy $E_0=1/2\ mV_0^2$, and conservation of total energy in the simulation is verified at each time instant with maximum error <0.1% (color figure online)



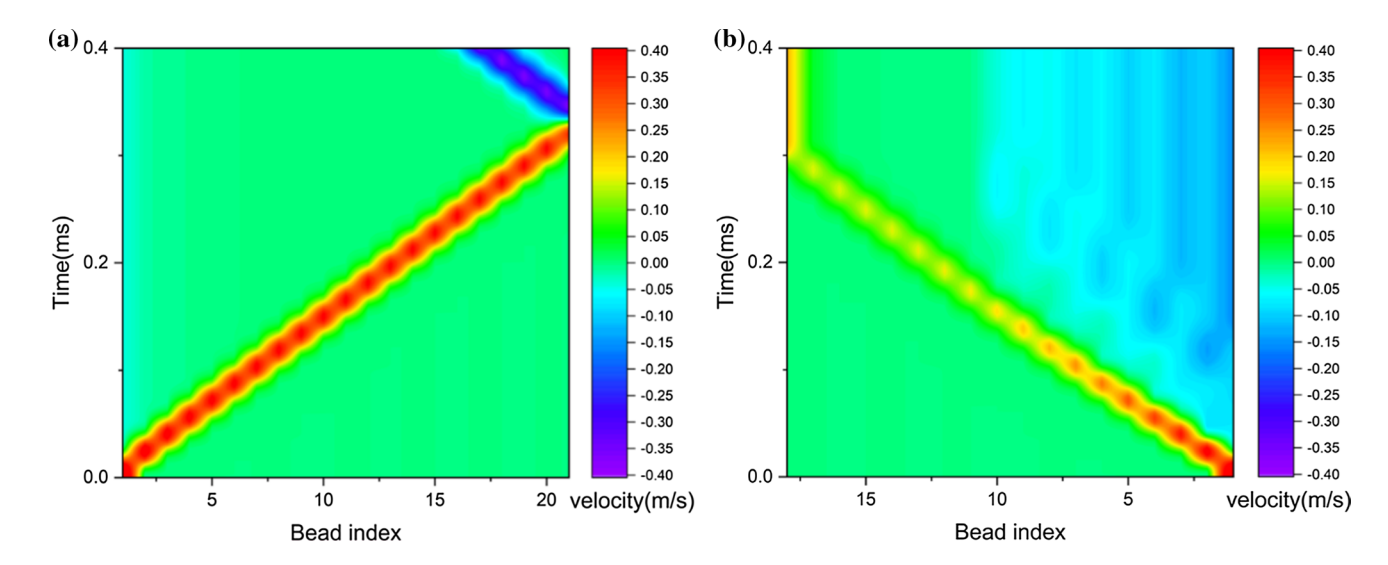


Fig. 8 Spatiotemporal evolutions of the velocities of the axial granules of the main lattice of the granular channel: **a** a Nesterenko solitary pulse is generated in the downstream configuration with small energy dissipation and then reflected back by the fixed lower end; **b**

a pulse with rapidly decaying magnitude is generated in the upstream configuration, and the end (upper) granule is in free flight as the primary pulse reaches the upper free boundary

the model that incorporates rotational and dissipative effects are presented as examples. In Fig. 7 we depict the instantaneous kinetic and potential energies of the granular network, as well as the dissipated energies due to viscous and friction effects. For the same configurations the spatiotemporal evolutions of the velocities of the axial granules are depicted in Fig. 8.

For the case of downstream pulse propagation, it can be noted that the impulsive energy is mainly partitioned into kinetic and potential energies (cf. Fig. 7a), which is the typical pattern featured in the propagation of the Nesterenko solitary pulse in a 1D homogeneous granular lattice with no side granules [1, 4, 5]. Meanwhile, the energy dissipated by friction is zero, denoting non-existence of rotational effects in this case, with all energy loss being caused by the viscolelastic dissipative effects. Indeed, in this case as the solitary pulse arrives at the site of an axial granule and causes its forward motion, there is no collision with the neighboring side granules due to the existence of the clearance. It can be concluded that the granular channel in its downstream configuration behaves like a 1D homogeneous granular lattice which supports the propagation of solitary pulses (cf. Fig. 8a), and the side granules play no role in the acoustics; it means that pulse propagation in the downstream configuration is independent of the number of pairs of side granules.

In the case of upstream pulse propagation, however, the existence of the side granules significantly affects the non-linear acoustics, causing rapid decrease of the magnitude of the transmitted pulse as parts of its energy "leak" to the side granules as it passes through their sites (cf. Fig. 8b). In this case there are rotations of the side granules (but not of

the axial granules), and as indicated in the plot of Fig. 7b frictional effects dissipate as much as 26% of the total input energy; at the same time viscous effects dissipate a mere 5.6% of the total input energy, which highlights the significant role played by the rotational and frictional effects. Predictably, the frictional moments on the side granules cause the transmission of a portion of the input energy to the rotational dynamics of side granules. Actually, in this case, about 2.85% of the input energy is retained by the side granules in the form of rotational kinetic energy. Moreover, there is a slowing down of the primary pulse in this case, which also highlights the strong dispersion of energy among the granules of the channel, since the speed of the highly nonlinear solitary pulse decreases with decreasing energy [1].

The comparisons between the numerical results and the experimental data, as well as the energy conservation within the granular channel that was demonstrated in the previous simulations elucidate the validity and accuracy of the developed numerical model, which provides us with a reliable tool for precise modeling and predictive design of the acoustics of 2-D granular networks. In the next section we apply this tool to highlight nonlinear acoustic non-reciprocity in an extended version of the inclined granular channel.

4 Acoustic non-reciprocity in the granular channel

The discussion in Sect. 3 has shown that pulse propagation behavior in the 2D inclined granular channel can be highly non-reciprocal and depends on the point of application of the



applied impulse. Hence, the nonlinear acoustics can switch from a downstream solitary pulse to an upstream rapidly decaying pulse, depending on the "activation" of the side granules which can absorb and locally dissipate a significant portion of the energy of the primary propagating pulse. Moreover, it is the asymmetric topology of the periodic clearances that gives rise to this acoustic non-reciprocity. It follows that a natural extension of our study is to employ the interesting acoustical features of the previous inclined granular channels to achieve a "diode-like" granular device that supports only one-way tunable (with energy) pulse propagation.

In this section, we present a simple, practically realizable extension of the granular channel depicted in Fig. 1 in the form of a 2D granular network with diode-like behavior. The network is shown in Fig. 9. Adopting the previous nomenclature, it contains 33 identical spherical granules of which 13 are axial granules—forming the homogeneous main lattice—and the remaining form 10 pairs of side granules. The granules are assembled in an inclined channel with adjustable width greater than $2\sqrt{3R+2R}$, which permits the existence of a periodic series of asymmetric clearances between the side granules and the axial beads, as discussed previously. The angle θ and the size of the clearances can be simply controlled by altering the width of the channel, with this relationship being depicted in Fig. 10. There are two limiting values for θ : At the lower limiting value $\theta = 60^{\circ}$ the clearances have zero widths, whereas at the upper limiting value $\theta = 90^{\circ}$ the side granules have no effect on the

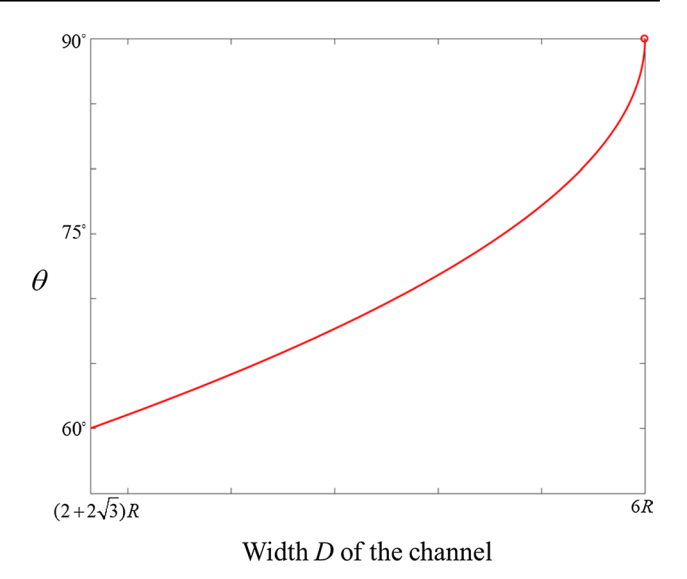
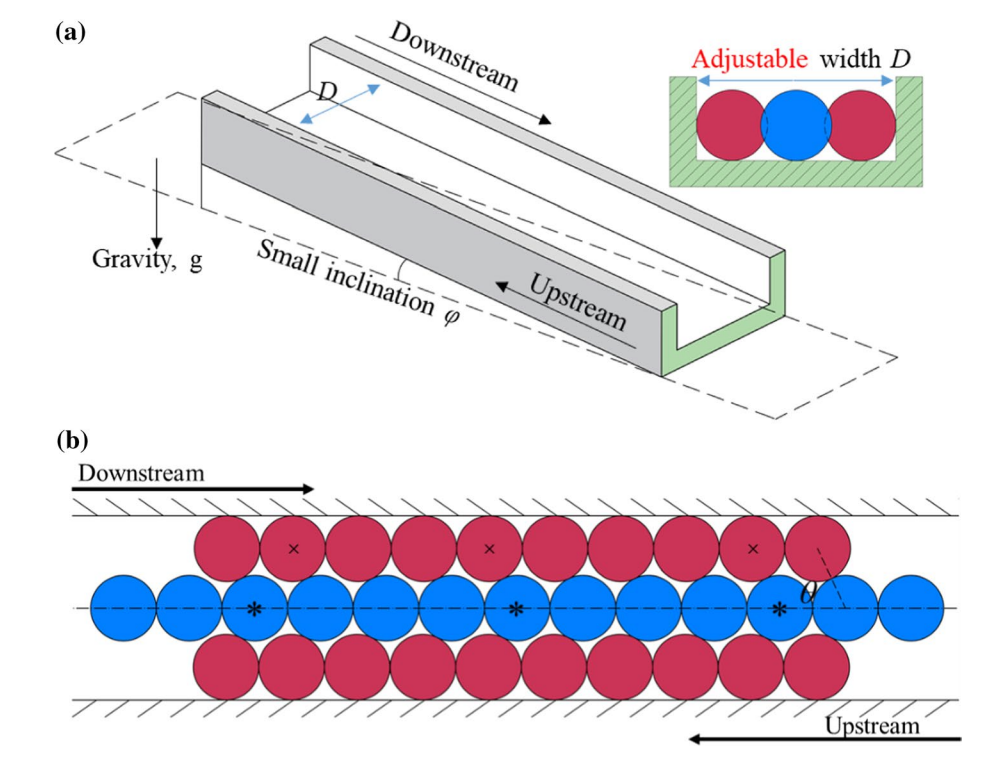


Fig. 10 The relationship between the width D of the channel and the angle θ : By adjusting the width, θ as well as the tolerance can be controlled (the clearance asymmetry in the channel can be "turned off" by setting $D = (2 + 2\sqrt{3})R$ corresponding to the lower limiting value $\theta = 60^{\circ}$)

motions of the axial granules. Moreover, a new feature of this network compared to that considered in the previous section is that now the side granules are also in contact with their neighbouring side granules (that is, in addition to the axial granules), which makes it possible for solitary wave propagation in the arrays of the side granules.

Fig. 9 Schematic of the nonreciprocal granular channel: a teflon base with adjustable width and cross-sectional view of the granules in the channel, and **b** top view of the granular channel topology; free ends are considered, and to test non-reciprocity the impulse is applied to either one of the boundary granules of the main homogeneous granular lattice; the velocities of the axial granules marked by stars (*) and the side granules marked by crosses (\times) are considered in Figs. 13 and 14





A slight tilt of the device at one of its ends (i.e., giving it a small inclination angle) produces the two distinct downstream and upstream configurations discussed in the previous section (cf. Fig. 9b). In this case, the component of gravity acting along the small slope can provide a small but sufficient force to ensure the stability of both configurations in their static condition, while it is negligible in the nonlinear acoustics considering the small inclination. Under impulse excitation the primary pulse in the upstream channel configuration will collide with the side granules and continuously transfer energy to them, which results in a rapidly decaying pulse propagating along the axial granular lattice. However, in the downstream channel configuration the side granules will not be excited by the propagating primary pulse which again will be in the form of the Nesterenko solitary pulse; hence, the granular channel will behave like a 1D homogeneous granular lattice which supports a higher amplitude primary propagating pulse. In other words, non-reciprocal pulse propagation will be realized, which depends solely on the direction of the pulse propagation, i.e., on which of its free ends is the main homogeneous granular lattice excited by the impulse.

We now proceed to study non-reciprocal pulse transmission in the granular channel for varying initial velocities of the end granules of the main lattice, in the range 0.1 m/s $\leq V_0 \leq$ 3.0 m/s. The material and geometric parameters of the granules are identical to those of the previous section, as is the angle $\theta=61^\circ$ (cf. Fig. 9b). The selected range of initial velocities ensured that the elastic strains of the granules and contact forces during granular interactions are within the elastic limit of the material and fulfilled the requirements of the Hertz contact law, respectively. All interaction forces between axial and side granules during primary

pulse propagation are estimated to be orders of magnitude larger than the component of gravity along the slope of the channel so that gravity effects can be safely ignored.

In Figs. 11 and 12 we consider primary pulse transmission in the downward and upward directions for impulses applied to the upper and lower granules, respectively, of the homogeneous main lattice. The initial velocity of the excited granules following the application of the impulse is equal to $V_0 = 1$ m/s. In these plots we study the energy partition of the primary pulse in each case, as well as the spatiotemporal velocity evolutions of the axial granules. In addition, the velocity profiles of selected axial granules situated in the main lattice (cf. Fig. 9) along the direction of wave propagation are shown in Fig. 13, while the velocities of all axial granules at the end of the simulation period (after which the axial granules are in free flight) for both upstream and downstream configurations are compared in Fig. 14. Moreover, the corresponding animations of energy transmissions and motions of the granules during pulse transmission are now included in the Supplementary Material (see SM videos). The non-reciprocal, direction-dependent primary pulse transmission in the granular channel is evident. Indeed, in the downstream direction (cf. Figs. 11a, 12a), a Nesterenko solitary wave is generated since the side granules have no effects on the nonlinear acoustics. The measured velocities (cf. Fig. 13—solid lines) exhibit the typical shape of the Nesterenko solitary wave, featuring a single-humped waveform with fast decaying tails [1, 37]. As the solitary propagates, the peak velocity of the corresponding granule slightly decreases due to the dissipative effect of damping. Eventually the last (13th) granule of the main lattice carries away 90% of the input energy in the form of kinetic energy with escape velocity equal to 0.95 m/s (cf. Fig. 14).

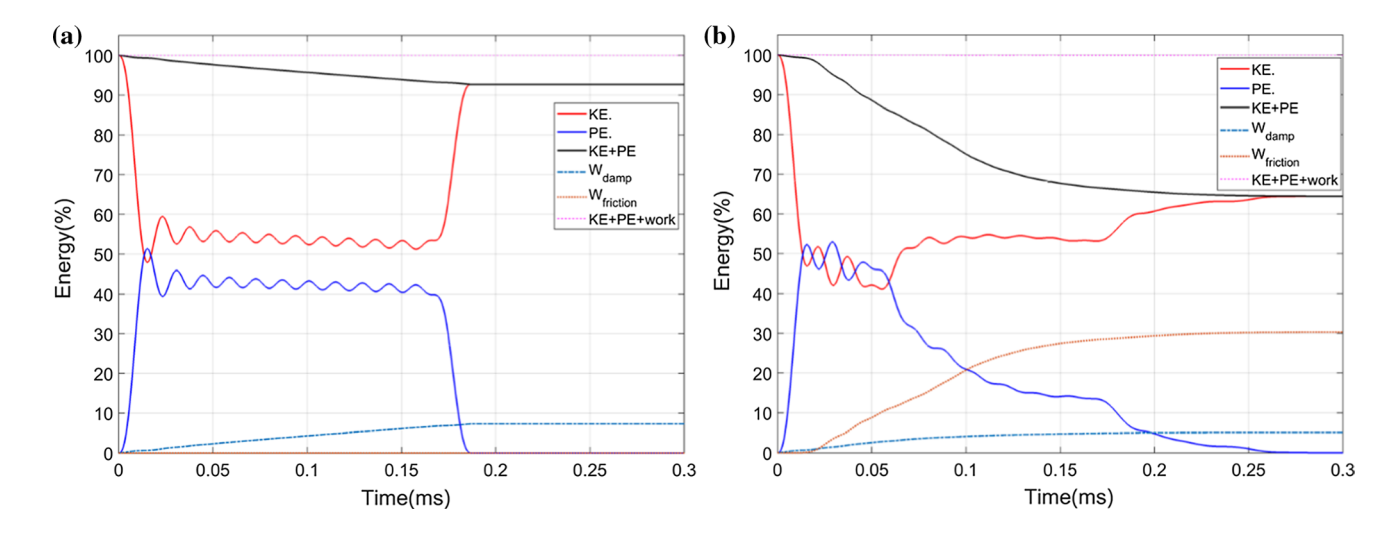


Fig. 11 Energy partition in the granular channel for **a** downstream and **b** upstream primary pulse propagation for $V_0 = 1$ m/s and $\theta = 61^\circ$; each energy component is normalized by the input energy

 $E_0 = 1/2 \ mV_0^2$, and conservation of total energy in the simulation has maximum error < 0.1% (the notation of Fig. 7 holds)



20 Page 12 of 16 Q. Zhang et al.

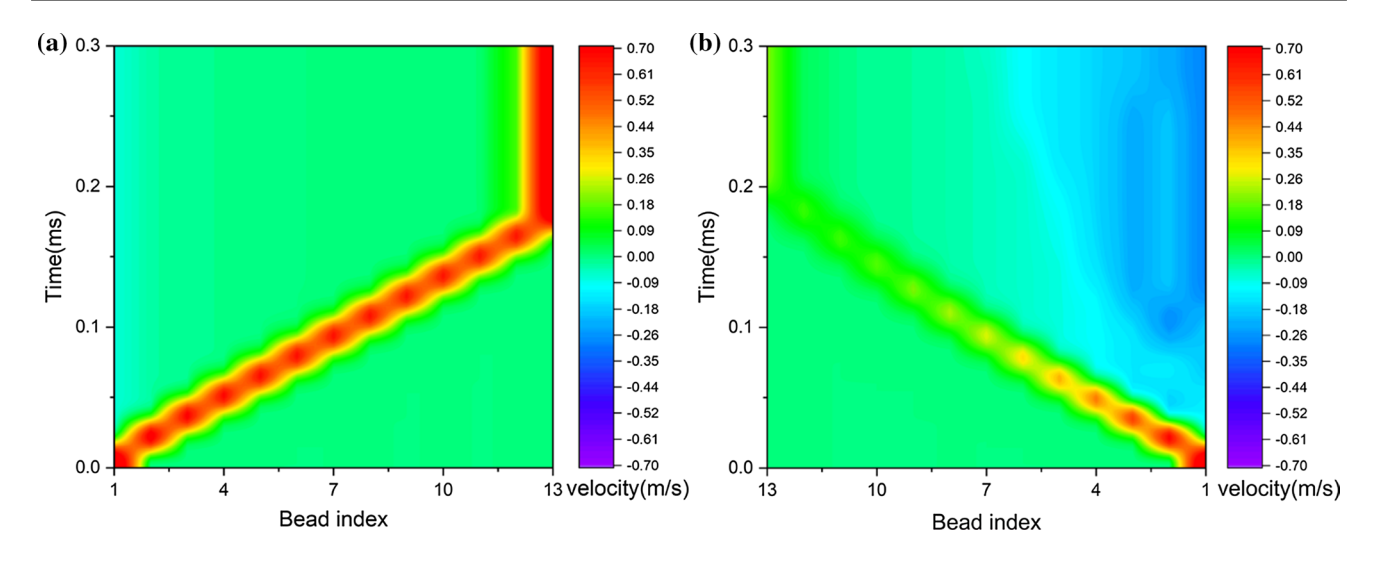


Fig. 12 Spatiotemporal evolution of the instantaneous velocities of the axial granules in the non-reciprocal granular channel for $V_0 = 1$ m/s and $\theta = 61^\circ$: **a** Nesterenko solitary pulse with nearly preserved amplitude is propagating in the downstream direction with

small energy dissipation; **b** strong energy dissipation of the propagating pulse in the upstream direction as its energy continuously leaks to the side granules (note near-extinction of the pulse in this case)

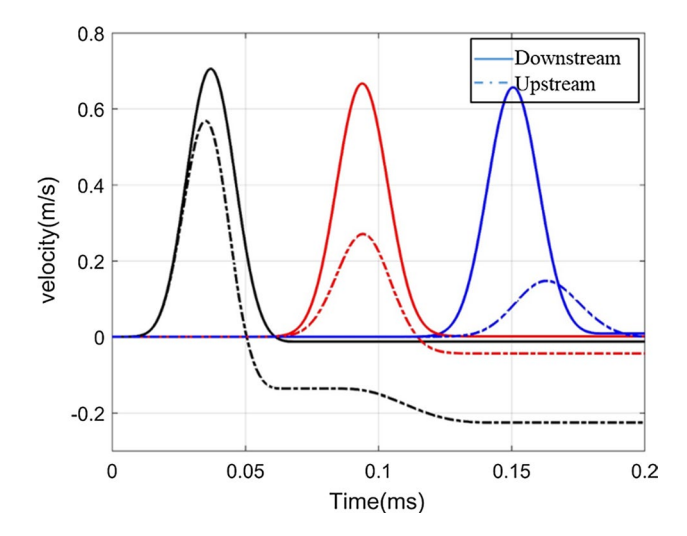


Fig. 13 Velocity profiles of the selected axial particles marked by stars in Fig. 9 for $V_0=1$ m/s and $\theta=61^\circ$; downstream primary pulse propagation corresponds to solid curves, and upstream to dash-dotted curves

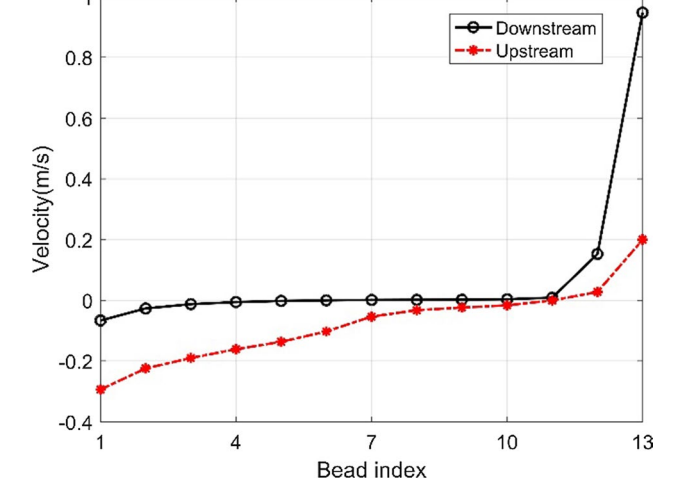


Fig. 14 Velocities of all axial granules at the end of the simulation period for $V_0 = 1$ m/s and $\theta = 61^{\circ}$ for downstream (black solid line) and upstream (red dash line) primary pulse propagation (color figure online)

Conversely, in the upstream direction, strong attenuation of the primary pulse is deduced (cf. Fig. 12b) as intense interactions with the side granules drain a large fraction of the transmitted energy from the axial lattice. This energy is either dissipated (35.5% of input energy) by friction, or is transformed into kinetic energy of the side granules, being continuously reflected back into the axial lattice in the form of kinetic energy with "negative" velocities (cf. Figs. 12b, 13, 14). As a result, the maximum velocity of the axial granules decreases significantly as the primary pulse propagates along the main lattice, while the escape velocity of the last

(13th) granule of the main lattice is relatively small (less than 0.2 m/s). This highlights the diode-like behavior of the non-reciprocal granular channel of Fig. 9. Apart from their smaller amplitudes, the responses of the axial granules for upstream propagation obviously lag behind their counterparts for downstram propagation (cf. Fig. 13), denoting a slowing down of the primary pulse and highlighting the strong dispersion of energy in the main lattice; this is explained by the fact that the speed of the highly nonlinear pulse has a strong dependence on energy.



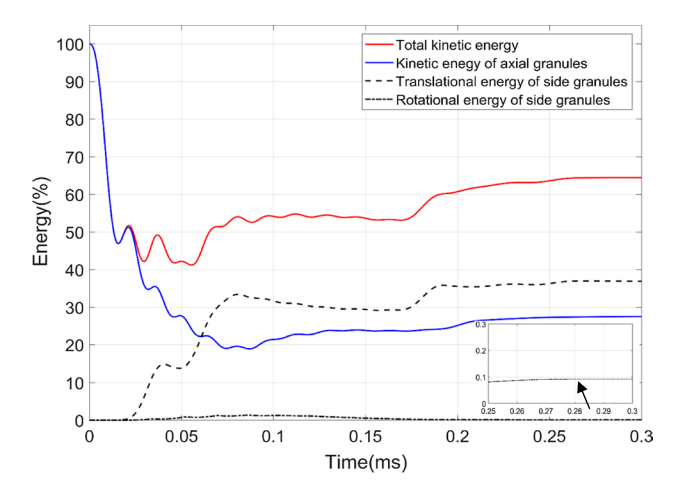
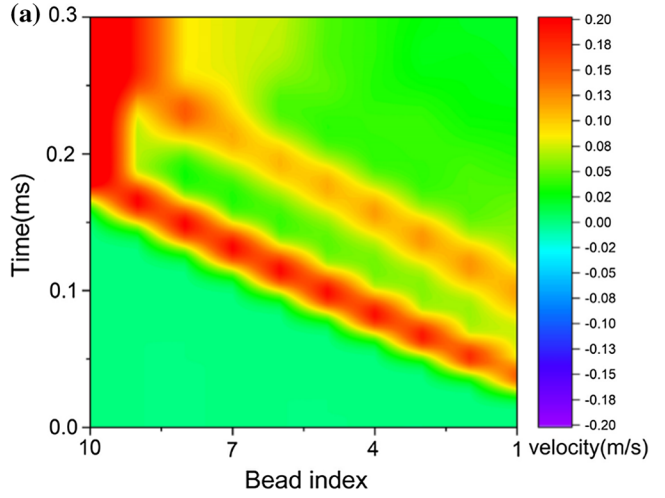


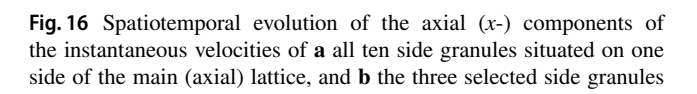
Fig. 15 Partition of the total kinetic energy of the granular channel for upstream pulse transmission for $V_0=1~\rm m/s$ and $\theta=61^\circ$: The kinetic energy of axial granules is denoted by the blue solid curve, the translational kinetic energy of the side granules by the black dashed line, and the rotational energy of side granules by the black dashedotted line; all energies shown are normalized by the input energy and the detail shows the steady state value reached by the rotational kinetic energy of the side granules from 0.25 to 0.3 ms

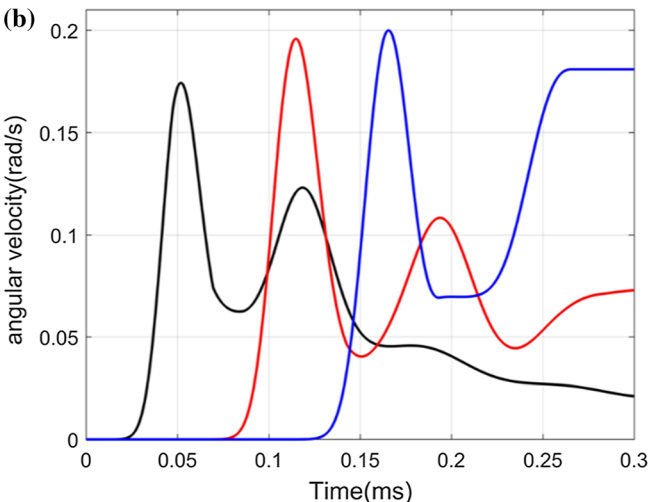
To show the strong influence of the side granules on the upstream primary pulse transmission, in Fig. 15 we detail the amount of kinetic energy retained in the axial lattice, as well as the kinetic energy captured in the side granules for upstream pulse propagation. In Fig. 16 we depict the spatiotemporal evolution of the velocity components in the axial (x-) direction of the side granules. Apart from the energy dissipated (35.5%) of the input energy) mainly due to frictional effects, we note that the side granules capture

as much as 37% of the input energy in the form of kinetic energy, which is more than the amount retained by the main (axial) homogeneous lattice (which captures about 27% of the input energy). In fact, among the energy retained in the main lattice, only about 4% of the input energy is transimmited up to the end of the channel by the primary pulse, while the remaining 23% of the retained energy is eventually reflected back (cf. Fig. 14) partly by the side spheres. Meanwhile, it is worth mentioning that the rotational energy of the side granules reaches its maximum at around 0.1 ms due to the torques caused by the frictional forces, and then begins to decrease until it reaches a small (but non-zero) constant level. As the primary pulse propagates, the upper side granules, while in contact with each other, are forced to rotate counter-clockwise by the strong interaction forces applied by the axial granules. Subsequently, the resulting friction torques generated as neighboring in-contact side granules rotate in the same direction, dissipate a part of their rotational energy. More interestingly, it can be observed that two solitary waves are generated in the side granular lattices, while the amplitude of the first solitary wave increases as it propagates, indicating that the side granules can continuously "drain" the transmitted energy from the axial lattice.

To quantify the acoustic non-reciprocity that occurs in the granular channel, in Fig. 17 we compare the output velocities of end axial granules (viewed as system outputs) in the downstream and upstream configurations with varying initial velocity V_0 of the impulsively excited granules (viewed as system inputs). From an energy perspective, the end granule for downstream pulse propagation can retain nearly 90% of the input energy, while less than 4% of the input energy is transmitted to its counterpart in the upstream







marked by crosses in Fig. 9, for $V_0 = 1$ m/s, $\theta = 61^{\circ}$ and upstream pulse propagation; the formation of two distinct solitary waves in the axial direction is clear



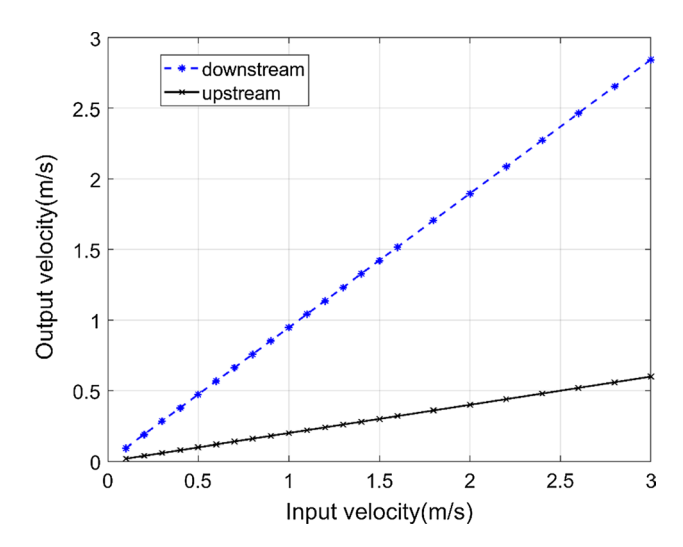


Fig. 17 Acoustic non-reciprocity in the granular channel: Output velocities of the end granules in the downstream and upstream configurations for varying input velocity V_0 and $\theta = 61^\circ$; the output velocity is measured at the end of each simulation after which the end granule is in free flight and will never interact again with its neighboring other axial granule

pulse propagation. It can be concluded that the nonlinear acoustics of this system is substantially dependent on the direction of pulse transmission.

As mentioned previously, the acoustic non-reciprocity of the granular channel is solely due to geometric effects or, more specifically, to the periodic series of symmetry-breaking clearances between the side granules and the axial granules of the main homogeneous lattice. Interestingly enough, this non-reciprocity can be tuned (and even completely eliminated) by simply varying the width of the channel, or, equivalently, by varying the angle $\theta \ge 60^{\circ}$ (cf. Fig. 9b). In turn, this controls the widths of the periodic clearances and tunes the acoustic non-reciprocity in the system. We note that the case $\theta = 60^{\circ}$ corresponds to the perfectly symmetric granular network which is reciprocal, as in that case all clearances are eliminated (cf. Fig. 10). It follows that nonlinear acoustic non-reciprocity in the granular channel can be tuned both by energy (i.e., varying the intensity of the applied impulse) as well as by the width of the channel (i.e., by varying the angle θ , and, hence, the widths of the clearances).

To highlight the tunability of the nonlinear acoustic non-reciprocity with respect to the angle θ (or the width of the granular channel), in Fig. 18 we depict the output velocities of the last granules in both configurations for varying angle $60^{\circ} \leq \theta < 90^{\circ}$ and fixed input velocity $V_0 = 1$ m/s. For the reciprocal case $\theta = 60^{\circ}$, predictably the two configurations yield the same result, but a small increase in θ breaks the acoustic reciprocity in the system. For downstream pulse transmission when θ is sufficiently small ($<60.05^{\circ}$ in this case) the

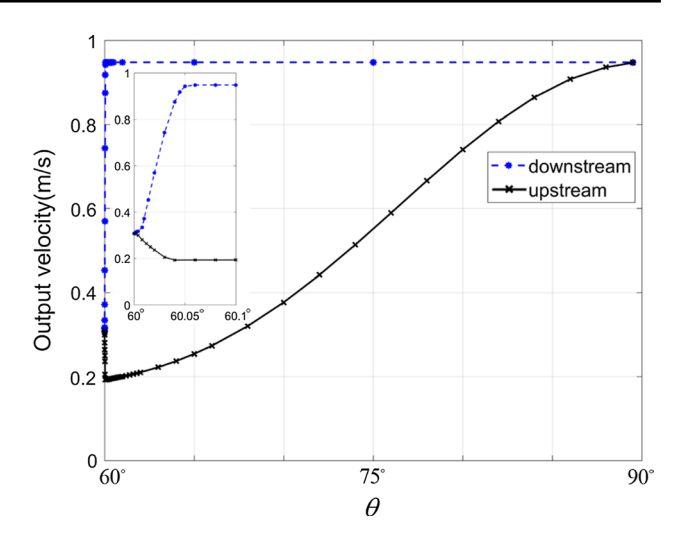


Fig. 18 Acoustic non-reciprocity in the granular channel: Output velocities of the end granules in the downstream and upstream configurations for input velocity $V_0=1$ m/s and $60^\circ \le \theta < 90^\circ$; the output velocity is measured at the end of each simulation after which the end granule is in free flight and will never interact again with its neighboring other axial granule; inset shows a detail of the results for $60^\circ \le \theta < 60.1^\circ$

widths of the clearances are quite small, so some of the axial granules can interact with the side granules during primary pulse propagation, leading to energy leaking to the side granules. However, the larger the clearance, the less energy leaks to the side granules, and therefore higher output velocity is achieved. Moreover, when $\theta > 60.05^{\circ}$ it is no longer possible for the axial granules to collide with the side granules within the considered time window, and the output velocity remains constant regardless of the varying angle; this is the case of Nesterenko solitary pulse propagation in the downstream direction. Non-reciprocity is eliminated at the higher limiting value $\theta = 90^{\circ}$ where the side granules cease to interact with the axial ones.

Similarly, for upstream pulse transmission and $\theta < 60.05^{\circ}$ the side granules can interact with their rear axial granules and transfer a part of their energy to the axial lattice. Accordingly, the output velocity decreases with increasing θ at first. However, for $\theta > 60.05^{\circ}$ the clearances are sufficiently large so that the side granules retain their energies without transferring any energy to the main lattice. In this case, the primary interaction between the axial granules and the side ones dominate the upstream pulse propagation, and the angle θ plays an important role. Understandably, in two-granule collisions, the larger the incident angle θ , the more energy will remain in the incident granule. Hence, the increase in θ yields an increase in output velocity until θ gets close to the other limiting value of 90° after which the side granules have no influence on the primary pulse propagation. It is worth mentioning that the "critical" angle (around 60.05° in this case) is dependent on the input velocity.



Additional animations of energy transmissions and motions of the granules during upstearm and downstream pulse transmission can be found in the Supplemental Information [40]. These results highlight further the non-reciprocal granular dynamics of the system considered.

5 Concluding remarks

In this study, we numerically examined pulse transmission in an inclined 2D granular channel composed of a main homogeneous uncompressed granular lattice with several pairs of side granules. This system was first studied in [33]. Assuming that all spherical granules are identical and depending on the width of the channel, it is possible to induce a symmetry-breaking periodic array of clearances between the side granules and some of their neighboring granules in the main lattice. In turn, these clearances yield interesting non-reciprocal phenomena in the nonlinear acoustics of this system under impulsive excitation. Given that the asymmetrically placed clearances yield two distinct channel configurations, namely a downstream and an upstream configuration, the channel supports either Nesterenko solitary pulses that transmit downstream or strongly decaying pulses that transmit upstream. In the latter case, a significant amount of energy gets continuously transferred from the main lattice to the side granules as the primary propagating pulse in the main lattice propagates upstream. It follows that the passive diodelike granular channel considered is doubly tunable not only by energy, as are all granular networks due to their strongly nonlinear dynamics and acoustics, but also by adjusting the width of the channel, i.e., by varying the size of the clearances and changing the level of asymmetry. Hence, the proposed system provides an interesting framework for studying strongly non-reciprocal acoustics in a strongly nonlinear acoustical system.

To accurately model and study the acoustics of this system we developed a mathematical model of the 2D granular network that takes into account the rotational dynamics of the granules, friction effects and material damping of the granule material. This model is a variant of the similar models presented in [31, 38, 39]. We validated the 2D granular model by revisiting the experimental results reported in [33] and showing much improved convergence compared with a dissipation-less prior model. The model enabled not only the detailed parametric study of nonlinear acoustic nonreciprocity in the granular channel with asymmetrically placed clearances, but also, through energy considerations, revealed the significant irreversible energy exchanges from the main lattice to the side granules for upward primary pulse transmission. In fact, it is precisely this continuous leaking of energy to the side granule pairs that causes nonreciprocity in the acoustics of the granular channel. This makes it possible to switch the type of pulse propagation in the granular network from a rapidly decaying pulse to a solitary pulse by simply changing the direction of pulse propagation and altering the lattice network topology.

The model and results herein contribute toward the predictive design of advanced acoustic granular devices capable of passively controlling mechanical energy flow. As such they may have important applications in engineering practice, e.g., as shock mitigators or diode-like logic elements in granular acoustic circuits. In addition, they may lead to better modeling and predictive design methods for granular interfaces and for 2D acoustic topologies such as branched granular networks, the interesting properties of which have been studied in previous works with modeling based on simplified effective particle-type models.

Acknowledgements This work was supported in part by the China Scholarship Council (CSC No. 201706160084), which funded the visit of Qifan Zhang to the University of Illinois at Urbana—Champaign, and by the National Science Foundation EFRI Grant No. 1741565. Any opinions, findings and conclusions or recommendations expressed in this material are those of the authors and do not necessarily reflect those of the National Science Foundation. The authors would like to acknowledge the constructive and highly insightful comments of two unknown reviewers, that contributed to the improvement of the manuscript.

Compliance with ethical standards

Conflict of interest The authors declare that they have no conflict of interest.

References

- 1. Nesterenko, V.F.: Dynamics of Heterogeneous Materials. Springer, New York (2001)
- Nesterenko, V.F.: Waves in strongly nonlinear discrete systems. Philos. Trans. R. Soc. A 376, 20170130 (2018)
- Nesterenko, V.F.: Solitary waves in discrete media with anomalous compressibility and similar to "sonic vacuum". J. Phys. IV 4(C8), 729-734 (1994)
- Sen, S., Hong, J., Bang, J., Avalos, E., Doney, R.: Solitary waves in the granular chain. Phys. Rep. 462, 21-66 (2008)
- Nesterenko, V.F.: Propagation of nonlinear compression pulses in granular media. J. Appl. Mech. Tech. Phys. 24, 733–743 (1983)
- Potekin, R., Jayaprakash, K.R., McFarland, D.M., Bergman, L.A., Vakakis, A.F.: Experimental study of nonlinear resonances and anti-resonances in granular dimer chains. Exp. Mech. 53, 861–870
- 7. Jayaprakash, K.R., Starosvetsky, Y., Vakakis, A.F.: A new family of solitary waves in granular dimmer chains with no pre-compression. Phys. Rev. E 83, 036606 (2011)
- 8. Coste, C., Falcon, E., Fauve, S.: Solitary waves in a chain of beads under Hertz contact. Phys. Rev. E **56**(5), 6104 (1997)
- Zhang, Q., Potekin, R., Li, W., Vakakis, A.F.: Nonlinear wave scattering at the interface of granular dimer chains and an elastically supported membrane. Int. J. Solids Struct. 182-183, 46-63 (2020)



20 Page 16 of 16 Q. Zhang et al.

 Starosvetsky, Y., Vakakis, A.F.: Traveling waves and localized modes in one-dimensional homogeneous granular chains with no pre-compression. Phys. Rev. E 82(2), 026603 (2010)

- Jayaprakash, K.R., Starosvetsky, Y., Vakakis, A.F.: Strongly nonlinear traveling waves in granular dimer chains. Mech. Syst. Signal Proc. 39, 91–107 (2012)
- Zhang, Y., Hasan, M.A., Starosvetsky, Y., McFarland, D.M., Vakakis, A.F.: Nonlinear mixed solitary—shear waves and pulse equi-partition in a granular network. Physica D 291, 45–61 (2015)
- Hasan, M.A., Cho, S., Remick, K., McFarland, D.M., Vakakis, A.F., Kriven, W.M.: Experimental study of nonlinear acoustic bands and propagating breathers in ordered granular media embedded in matrix. Granul. Matter 17, 49–72 (2015)
- Hasan, M.A., Starosvetsky, Y., Vakakis, A.F., Manevitch, L.I.: Nonlinear targeted energy transfer and macroscopic analogue of the quantum Landau-Zener effect in coupled granular chains. Physica D 252, 46–58 (2013)
- Starosvetsky, Y., Jayaprakash, K.R., Vakakis, A.F.: Scattering of solitary waves and excitation of transient breathers in granular media by light intruders and no pre-compression. J. Appl. Mech. 79, 011001 (2012)
- Zhang, Z., Manevitch, L.I., Smirnov, V., Bergman, L.A., Vakakis, A.F.: Extreme nonlinear energy exchanges in a geometrically nonlinear lattice oscillating in the plane. J. Mech. Phys. Solids 110, 1–20 (2018)
- Zhang, Z., Koroleva, I., Manevitch, L.I., Bergman, L.A., Vakakis, A.F.: Non-reciprocal acoustics and dynamics in the in-plane oscillations of a geometrically nonlinear lattice. Phys. Rev. E 94(3), 032214 (2016)
- Spadoni, A., Daraio, C.: Generation and control of sound bullets with a nonlinear acoustic lens. Proc. Natl. Acad. Sci. 107(16), 7230–7234 (2010)
- Donahue, C.M., Anzel, P.W.J., Bonanomi, L., Keller, T.A., Daraio,
 C.: Experimental realization of a nonlinear acoustic lens with a tunable focus. Appl. Phys. Lett. 104(1), 014103 (2014)
- Melo, F., Job, S., Santibanez, F., Tapia, F.: Experimental evidence of shock mitigation in a Hertzian tapered chain. Phys. Rev. E 73(4), 041305 (2006)
- 21. Hong, J.: Universal power-law decay of the impulse energy in granular protectors. Phys. Rev. Lett. **94**, 108001 (2005)
- Doney, R., Sen, S.: Decorated, tapered, and highly nonlinear granular chain. Phys. Rev. Lett. 97, 155502 (2006)
- 23. Lawney, B.P., Luding, S.: Frequency filtering in disordered granular chains. Acta Mech. 225, 2385–2407 (2014)
- Li, F., Anzel, P., Yang, J., Kevrekidis, P.G., Daraio, C.: Granular acoustic switches and logic elements. Nat. Commun. 5, 5311 (2014)
- Boechler, N., Theocharis, G., Daraio, C.: Bifurcation-based acoustic switching and rectification. Nat. Mater. 10, 665–668 (2011)

- Cui, J., Yang, T., Chen, L.: Frequency-preserved non-reciprocal acoustic propagation in a granular chain. Appl. Phys. Lett. 112, 181904 (2018)
- Plimpton, S.: Fast parallel algorithms for short-range molecular dynamics. J. Comput. Phys. 117(1), 1–19 (1995)
- Awasthi, A.P., Smith, K.J., Geubelle, P.H., Lambros, J.: Propagation of solitary waves in 2D granular media: a numerical study. Mech. Mater. 54, 100–112 (2012)
- Leonard, A., Chong, C., Kevrekidis, P.G., Daraio, C.: Traveling waves in 2D hexagonal granular crystal lattices. Granul. Matter 16, 531–542 (2014)
- Li, L., Yang, X., Zhang, W.: Two interactional solitary waves propagating in two-dimensional hexagonal packing granular system. Granul. Matter 20, 49 (2018)
- Yang, K., Sutton, M.: Nonlinear wave propagation in a hexagonally packed granular channel under rotational dynamics. Int. J. Solids Struct. 77(3), 65–73 (2015)
- Goldenberg, C., Goldhirsch, I.: Friction enhances elasticity in granular solids. Nature 435, 188–191 (2005)
- Pal, P.K., Waymel, R.F., Geubelle, P.H., Lambros, J.: Tunable wave propagation in granular crystals by altering lattice network topology. J. Eng. Mater. Technol. 139(1), 011005 (2016)
- Nishida, M., Tanaka, Y.: DEM simulations and experiments for projectile impacting two-dimensional particle packings including dissimilar material layers. Granul. Matter 12(4), 357–368 (2010)
- 35. Manjunath, M., Awasthi, A., Geubelle, P.H.: Wave propagation in 2D random granular media. Physica D **266**, 42–48 (2014)
- Waymel, R.F., Wang, E., Awasthi, A., Geubelle, P.H., Lambros, J.: Propagation and dissipation of elasto-plastic stress waves in two dimensional ordered granular media. J. Mech. Phys. Solids 120, 117–131 (2018)
- 37. Starosvetsky, Y., Jayaprakash, K.R., Hasan, M.A., Vakakis, A.F.: Topics on the Nonlinear Dynamics and Acoustics of Ordered Granular Media. World Scientific Press, Singapore (2017)
- Tsuji, Y., Tanaka, T., Ishida, T.: Lagrangian numerical simulation of plug flow of cohesionless particles in a horizontal pipe. Powder Technol. 71, 239–250 (1992). (29(1), 47–65, 1979)
- Cundall, P.A., Strack, O.D.: A discrete numerical model for granular assemblies. Géotechnique 29(1), 47–65 (1979)
- Supplementary Material for "Pulse Transmission and Acoustic Non-reciprocity in a Granular Channel with Symmetry-Breaking Clearances"

Publisher's Note Springer Nature remains neutral with regard to jurisdictional claims in published maps and institutional affiliations.

